Front. Phys. 11(3), 114701 (2016)
DOI 10.1007/s11467-015-0546-1

RESEARCH ARTICLE

Numerical investigation of relationship between water contact angle and drag reduction ratio of superhydrophobic surfaces

Liang Yin[1], Hai-Feng Zhang[1,2,†], Shu-Yuan Shi[1], Yao Lu[1], Yang Wang[1], Xiao-Wei Liu[1,2]

[1] *MEMS Center, Harbin Institute of Technology, Harbin 150001, China*

[2] *Key Laboratory of Micro-Systems and Micro-Structures Manufacturing (Ministry of Education), Harbin 150001, China*

Corresponding author. E-mail: †zhanghf@hit.edu.cn

Received August 1, 2015; accepted November 12, 2015

This paper proposes a novel bubble model to analyze drag reduction. The relationship between the slip length and air bubble height is discussed. The numerical relationship between the surface contact angle and slip length is obtained using the solid-liquid contact ratio in the Cassie equation. The surface drag reduction ratio increases by 40% at low velocities when the solid liquid contact ratio decreases from 90% to 10%. An experimental setup to study liquid/solid friction drag is reported. The drag reduction ratio for the superhydrophobic surface tested experimentally is 30%–35% at low velocities. These results are similar to the simulation results obtained at low velocities.

Keywords drag reduction, air bubble, slip length, fraction, superhydrophobic

PACS numbers 47.11.Fg, 68.08.De

1 Introduction

Drag reduction in fluid flow is a fundamental issue in the field of process engineering, and achieving drag reduction will benefit a multitude of industries [1, 2]. In nature, water-repelling surfaces of floating plants and semiaquatic insects allow them to effectively move on and in water, and breathe while submerged under water [3]. These properties result from the ability of some natural superhydrophobic surfaces to passively fix and retain an air film between water and the solid surface, thus reducing the solid surface area in contact with water. The surface minimizes the water-solid contact area, significantly reducing the frictional drag between water and the solid [4–8]. Therefore, the surprising performance of the superhydrophobic surface has attracted much attention of scholars and various drag reduction researches were conducted [9, 10].

Over the past decade, the fluidic drag reduction effect of superhydrophobic surfaces has been investigated both theoretically and experimentally. Friction drag reduction has been verified by theoretical, numerical, and experimental studies based on the slip hypothesis for both laminar and turbulent flows. The effect of slip has been validated through direct numerical simulation and theoretical prediction of the channel flow [11, 12]. For instance, Fukagata *et al.* theoretically predicted that drag reduction can be achieved by using superhydrophobic surfaces not only for laminar flows, but also for turbulent channel flows [13]. Lauga and Stone analyzed the slip velocity in channels by computational fluid dynamics [14]. Davies *et al.* used FLUENT to study the influence of roughness on pressure drop [15]. Cheng *et al.* numerically calculated the influence of the total shear-free area or the air-water interface area (area in which the slip effect occurs) and its dependency on the slip length [16]. However, these researchers did not consider the effect of surface roughness and wettability. In several experiments, it was found that even though invasion is one of the factors that affect slip length, the same liquid flowing along a surface with the same wettability will still result in a different slip length.

Many scientists have studied surface roughness, and it has been proved that it can suppress liquid slip on the microscale regardless of the microcosmic conditions. This paper proposes a novel bubble model. The relationship between the slip length and the air bubble height depending on the differences in air bubble height and surface roughness is discussed. The numerical relationship between the surface contact angle and slip length is derived. This relationship can help understand the drag reduction property of superhydrophobic surfaces.

2 Model and mathematical formulation

2.1 The bubble model

According to the Cassie model, micro air bubbles exist between the rough surface and liquid layer; this is the most important cause of drag reduction of the rough surface. This theory has been confirmed by several experiments conducted using microscopic instruments [17–21]. An air bubble model of the superhydrophobic surface has been proposed. Based on the N–S equation, it is assumed that the liquid flow velocity is not particularly high (i.e., the Reynolds number is less than 2000) to ensure that the fluid is in the advection flow state. Meanwhile, for the convenience of discussion and observation, only 2D models are considered. The theoretical model for a rough superhydrophobic surface is shown in Fig. 1(a). To simplify the local boundary conditions on a free surface, Fig. 1(a) can be considered to represent an air bubble model, as shown in Fig. 1(b). Here, the elliptical short shaft height h represents the bubble spike height because when the velocity is sufficiently small, it is reasonable to assume that bubbles are still in the rough surface structure of the slots.

2.2 Mathematical formulations

This model comprised three basic models. First, for steady-state incompressible laminar flows, the fluid flow can be described by a set of equations, including the continuity and momentum equations [22],

$$\rho\frac{\partial u}{\partial t}+\rho(u\cdot\nabla)u=\nabla\cdot[-pI+\eta(\nabla u+(\nabla u)^T)]+F,$$
$$\nabla\cdot u=0, \tag{1}$$

where u is the velocity (m/s); η is the dynamic viscosity (Pa·s); ρ is the density (kg/m^3); and p is the pressure (Pa). The volumetric force components F are set to zero

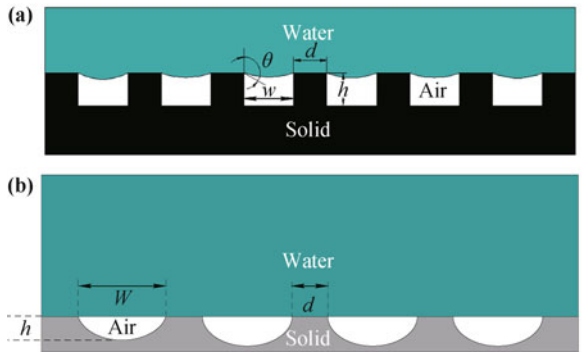

Fig. 1 **(a)** Theoretical model for a rough superhydrophobic surface. **(b)** Air bubble model.

in the model. In turbulent flows, the corresponding governing equations can be written as follows:

$$\rho\frac{\partial u}{\partial t}+\rho(u\cdot\nabla)u=\nabla\cdot[-pI+\eta_{eff}(\nabla u+(\nabla u)^T)]+F,$$
$$\nabla\cdot u=0. \tag{2}$$

The turbulent influences are taken into account by introducing effective viscosity η_{eff}, which is the sum of turbulent viscosity η_t and molecular viscosity η:

$$\eta_{eff}=\eta_t+\eta. \tag{3}$$

The second model used is the standard k–ε turbulence model. It is used in order to consider both laminar flow and turbulence.

$$\frac{\partial(\rho\varepsilon)}{\partial t}+\frac{\partial(\rho\varepsilon u_i)}{\partial x_i}=\frac{\partial}{\partial x_j}\left[\left(\mu+\frac{\mu_t}{\sigma_\varepsilon}\right)\frac{\partial\varepsilon}{\partial x_j}\right]+C_{1\varepsilon}\frac{\varepsilon}{k}(G_k+C_{3\varepsilon}G_b)-C_{2\varepsilon}\rho\frac{\varepsilon^2}{k}+S_\varepsilon,$$
$$\frac{\partial(\rho k)}{\partial t}+\frac{\partial(\rho k u_i)}{\partial x_i}=\frac{\partial}{\partial x_j}\left[\left(\mu+\frac{\mu_t}{\sigma_k}\right)\frac{\partial k}{\partial x_j}\right]+G_k+G_b-\rho\varepsilon-Y_M+S_k. \tag{4}$$

The third model is the RSM (Reynolds Stress Model). The RSM equation is written as follows:

$$\frac{\partial(\rho\overline{u_i'u_j'})}{\partial t}+C_{ij}=D_{T,ij}+D_{L,ij}+P_{ij}+G_{ij}+\Phi_{ij}-\varepsilon_{ij}+F_{ij}+S_{user}, \tag{5}$$

where $\frac{\partial(\rho\overline{u_i'u_j'})}{\partial t}$ is the local time derivative of the Reynolds stress, C_{ij} is the convection, $D_{T,ij}$ is the turbulent diffusion, $D_{L,ij}$ is the molecular diffusion, P_{ij} is the stress, G_{ij} is the buoyancy, Φ_{ij} is the pressure strain, ε_{ij} is the dissipation, F_{ij} is the volumetric force components, and S_{user} is the user-defined source term.

In this paper, the variational problem for the specific turbulent flow construction is resolved by using the standard k–ε turbulence model because of the following reasons. First, as the most commonly used turbulence model in CFD simulation, the standard k–ε turbulence model has been proved to be sufficiently accurate for predicting fluid flow [23]. Second, compared with sophisticated models, the standard k–ε model can be used to solve the variational problem more conveniently from the viewpoint of available computational resources.

3 Results and discussion

3.1 The influence of the slip length on bubble height

In order to estimate the effect of surface roughness on

friction drag reduction, we used the air bubble model to study the effects of different bubble heights on velocity distribution. We considered simplified local boundary conditions on the free surface: the micro air bubble was anchored at the edge of the microstructure, and it was shaped as a fixed spherical cap independent of stress. This approximation is valid in the limit of small capillary numbers. Figure 2(a) shows the velocity distribution of the micro channel flow. The slip length hypothesis was considered a basis for explaining friction drag reduction attributed to the slip of the flow over superhydrophobic surfaces. Many techniques to measure slip length have been developed to study flows on the surfaces [24, 25]. Navier's hypothesis states that the velocity on a surface is proportional to the velocity gradient on the surface $y = y_0$. This can be expressed as follows:

$$u(y=0) = \beta \frac{\mathrm{d}u}{\mathrm{d}y}\bigg|_{y=0}. \tag{6}$$

Here, β is the slip length, and $\mathrm{d}u/\mathrm{d}y$ is the shear rate or velocity gradient in the direction normal to the surface. The velocity at the wall, u $(y = 0)$, is called the slip velocity.

Figure 2(b) shows the velocity distribution along the direction normal to the surface with 10 μm air bubbles. It indicates that the velocity distribution near the sliding surface increased linearly, and hence, we can use Eq. (6) to calculate the effective slip length β. Figure 2(c) shows the curve of the slip length at different air bubble heights. The lower the bubble height, the larger was the slip length. The numerical results [Fig. 2(c)] clearly showed that slip length decreased with increase in air bubble height. Our result is a valid evidence of Steinberger's results, according to which a large decrease in the effective slip length was obtained for protruding menisci [26]. In other words, if a rough surface is smoothened and a very thin layer of air is maintained, the effective slip length is much larger than that under any other conditions. These numerical results show quantitatively that the boundary condition of a liquid flowing on a composite surface embedded with microbubbles depends greatly on the shape of the gas-liquid interfaces.Thus, it can be concluded that during the preparation of a superhydrophobic surface, adjusting the surface topography to make the gas-liquid contact area smooth can induce drag reduction of the surface.

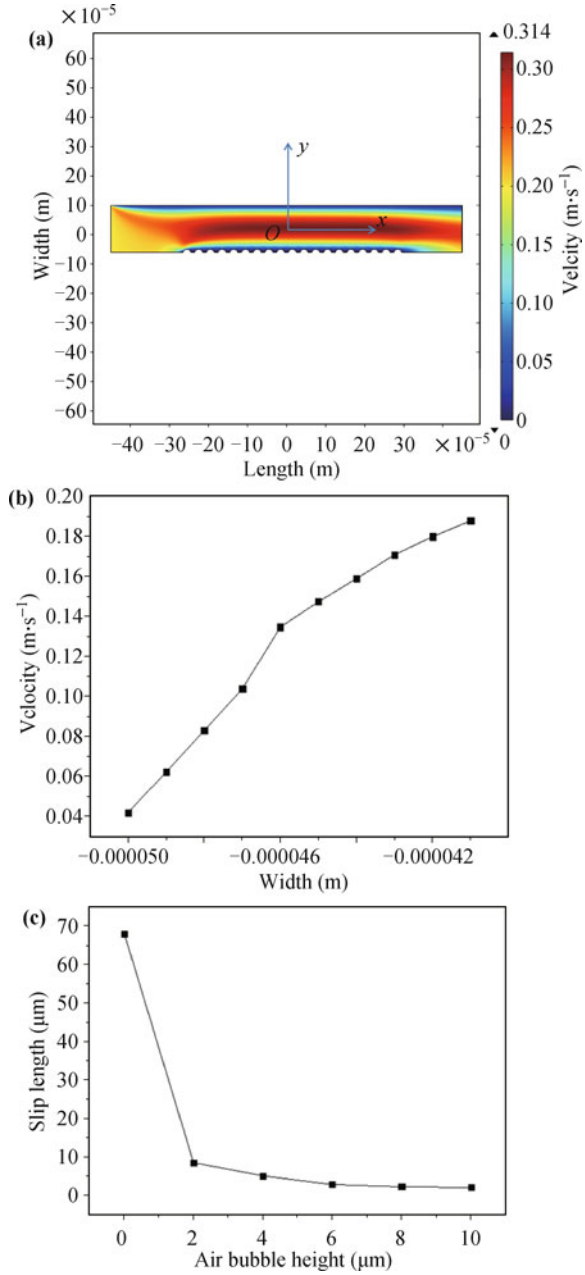

Fig. 2 **(a)** Velocity distribution of the micro channel flow. **(b)** Velocity distribution along the direction normal to the surface with 10 microns air bubble. **(c)** Curve of the slip length with different air bubble height.

3.2 Stability of air-water interface

The presence of entrapped gas in surface structuresis a necessary condition for realizing diverse superhydrophobic surfaces. Therefore, the key to superhydrophobic surface design is to entrap gas in the microstructures of a surface or to prohibit the transition from the Cassie to Wenzel state.

In this subsection, we study the condition under which the air water interface (meniscus) may transition from the nonwetted state (Cassie state) to the wetted state (Wenzel state). This is important in practical applications related to submerged bodies because once the thin gas layer is replaced by liquid, none of the beneficial effects remain. Lee and Kim adopted the latter approach

to develop an equation to determine the maximum allowable hydrostatic pressure in terms of the surface microstructure [27]:

$$p_{\max}\phi_g \leqslant \frac{-2\gamma\sqrt{\pi(1-\phi_g)\cos\theta}}{L} \tag{7}$$

where $P_{\max}$ is the maximum allowable pressure without transition, ϕ_g is the gas fraction, γ is the surface tension of the liquid (72×10^{-3} N·m in the case of water), θ is the contact angle, and L is the pitch (distance between two posts). Figure 3(a) schematically shows the microscopic contact state of the superhydrophobic surface underwater when the hydraulic pressure is less than the critical value P_c. Water was suspended on the top of the pillar, and the spaces within the pillar formed an air layer, indicating an air/water/ pillar (A/W/P) interface underwater. On the other hand, after the hydraulic pressure exceeded the critical value P_c, the waterpenetrated into the spaces within the pillar [see Fig. 3(b)], and the A/W/P interface did not exist under these conditions. Moreover, the existence of a multi-scale pillar increased the contact area between the water and solid surface, enhancing the total adhesion between the water and solid surface according to the smooth solid/liquid interface theory. Further, the pressure provided additional energy to eliminate the air layer. Therefore, the critical pressure P_c is a key factor affecting air layers in underwater superhydrophobic surfaces.

3.3 The influence of the contact angle on slip length

From the viewpoint of thermodynamics, the Cassie equation reveals the static solid-liquid contact relationship. It introduces the concept of solid-liquid contact ratio. In general, the superhydrophobic surface drag reduction reference model is the Cassie model. Further, the slip length is included in the Cassie equation and the expression for solid-liquid contact ratio. According to the equations of Cassie and Baxter, the roughness of the surface can change the wettability of the surface.

$$\cos\theta = f\cos\theta_0 + f - 1, \tag{8}$$

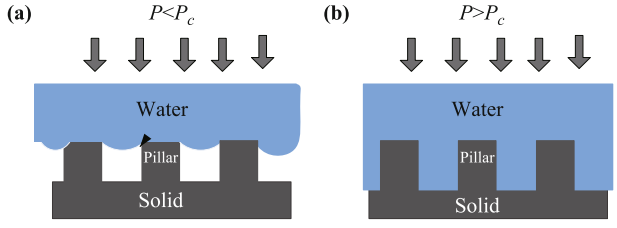

Fig. 3 **(a, b)** Model illustration to explain the states of air layer on solid surface under water when the hydraulic pressure P is below and above the critical value of P_c, respectively. A/W/P interface indicates the air/water/pillar interface.

where f is the ratio of the contact area of a droplet with micro-bumps to the total contact area, and θ and θ_0 are the contact angles for the real and ideal surfaces, respectively.

Based on Eq. (8), a 2D superhydrophobic surface model was built with different solid-liquid contact ratios. In a pipeline flow, a flow rate under a constant shear stress value or identical pressure difference between different pipelines could be used to evaluate the effect of drag reduction. In order to investigate the effect of solid-liquid contact ratio on slip length, equidistant distributed channels with 25 consecutive bulges each at their bottoms are established. The length and width of the microchannel are 1000 μm and 200 μm, respectively. The model is shown in Fig. 4(a). In order to discuss the model in the laminar flow states, the Renault coefficient must be less than 2000. The Renault coefficient is calculated as follows:

$$Re = \frac{\rho v d}{\mu}. \tag{9}$$

Here, d is the characteristic length of the pipes; v is the average speed of fluid flowing through a pipe; ρ is fluid density; and μ is the viscosity of the fluid. Under room temperature, the viscosity of water is 1.001×10^{-3} Pa·s^{-1} and the density is 1000 kg·m^{-3}. Thus from the above formula, it can be ensured that the maximum flow velocity is around 10 m·s^{-1} in a laminar flow state. In order to explore the relationship between the ratio of solid-liquid interface and slip length, water flow velocity is around 2 m·s^{-1}.

The boundary conditions are as follows: The bulges on the surface are the sliding surfaces. They are used to simulate liquid-gas interface. The no-sliding surface is used to simulate the solid-liquid interface. The normal vector inflow velocity is 2 m·s^{-1}. By changing the length of the bulge, the solid-liquid contact ratio is changed. A series of simulation results were obtained. Figure 4(a) shows the velocity profile of the solid-liquid contact ratio <10%. The effect of reducing solid-liquid contact ratio from 90% to 10% on the slip lengthis shown in Fig. 4(b). The relationship between the solid-liquid contact ratio and the slip length is discussed. Figure 4(b) shows that the lower the contact ratio, the longer is the slip length. Typically, Newtonian liquids undergo laminar flow across solid surfaces, when a surface is hydrophilic, the measured velocity profile is consistent with thesolution of Stokes's equation and well-accepted no-slipboundary condition. The velocityprofile is a parabola, as shown in Fig. 4(c). So the maximum flowrate is considered to be at the mid-point of the channel. The velocity profile on the superhydrophobic surface consisting of nanostructure and

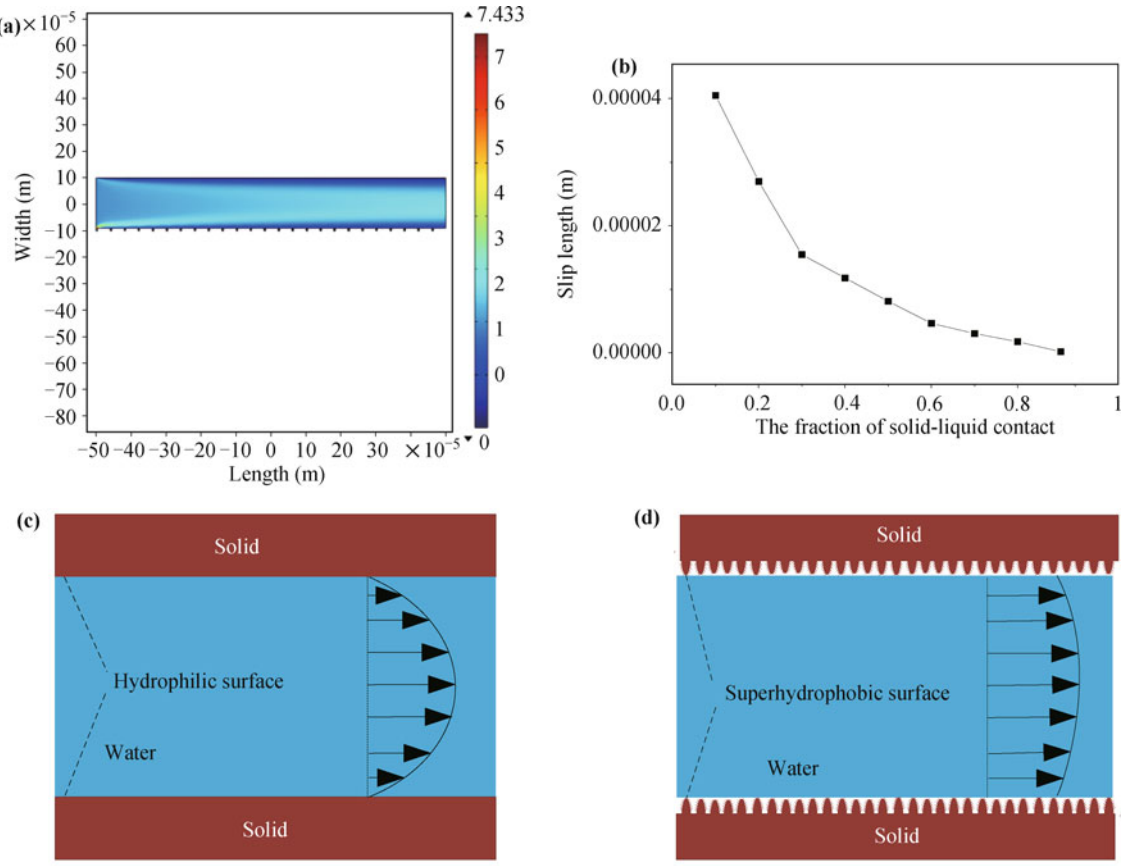

Fig. 4 **(a)** Velocity profile of the solid-liquid contact ratio under 10%. **(b)** Effect of solid-liquid contact ratio on the slip length. **(c)** Hydrophobic layer in a microchannel with no-slip boundary condition. **(d)** Superhydrophobic surface in a microchannel with a slip boundary condition.

airpockets on which fluid slip and nonzero velocity atthe surface is shown in Fig. 4(d). The presence of air pocketson the surface results in reduction of the solid surface area incontact with water, which in turn leads to frictional dragreduction.The transition from hydrophobic surface to superhydrophobic surface has obvious effect on the slip length as shown in Fig. 4(b). In addition, through numerical simulation and calculation, it was found that when the solid-liquid contact ratio was reduced from 90% to 10%, the surface drag reduction rate increased by 40%.

In order to discuss the relationship between the slip length and the solid-liquid contact ratio, we used linear fitting to obtain the relation function and the fitting curve. The curve in Fig. 4(b) can be fit using the following polynomial equation:

$$y_{\text{slip}} = 0.0002f^4 - 0.0005f^3 + 0.0005f^2 - 0.0003f + 6 \times 10^{-5}. \quad (10)$$

Here, y_{slip} is the slip length; f represents the solid-liquid contact ratio; and determination coefficient $R^2 = 0.9979$, which illustrates that the curve fitting degree is high and has high credibility.

By combining Eqs. (8) and (10), the following relation is obtained:

$$y_{\text{slip}} = 0.0002\left(\frac{\cos\theta+1}{1+\cos\theta_0}\right)^4 - 0.0005\left(\frac{\cos\theta+1}{1+\cos\theta_0}\right)^3 + 0.0005\left(\frac{\cos\theta+1}{1+\cos\theta_0}\right)^2 - 0.0003\left(\frac{\cos\theta+1}{1+\cos\theta_0}\right) + 6 \times 10^{-5}. \quad (11)$$

When $\cos(\theta_0) = 0.5$, 0.6, 0.7, and 0.8, the above polynomial equation can be represented as shown in Fig. 5.

It can be seen from Fig. 5 that when the contact angle is smaller than a certain value, the slip length is negative, which means that the surface undergoes resistance enhancement at this time. Hyvaluom also determined that the slip length on protruded bubbles decreased from a positive to negative value with decreasing water contact angle [28]. We showed that gas trapped in a solid surface can also act as an anti-lubricant and promote high friction. The liquid-gas menisci have a great influence on the boundary condition, and can transform the surface from a slippery one to a sticky one. This observation can

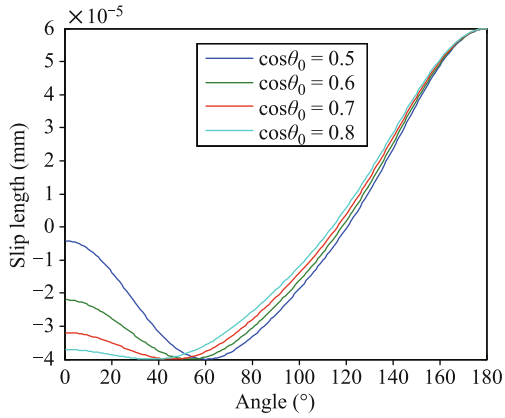

Fig. 5 Relationship between different θ_0 (Young's contact angle on an ideally flat surface) the slip length.

be explained by means of the theoretical predictions of Richardson [29, 30]. Our results support these predictions.

In addition, when the contact angle exceeded the critical value, the slip length increased with the contact angle. When the contact angle became 180°, indicating that the solid surface was completely superhydrophobic, the slip length did not become infinite but was several tens of micrometers. This suggests that even if the solid surface is completely superhydrophobic, the viscous resistance between the gas and liquid cannot be ignored. The critical value was calculated, and we found that different intrinsic critical angles of the surface correspond to different contact angles. The critical contact angle is about 100°–120° for roughness surface. It is therefore essential to integrate the control of the surface structure in fluidic microsystems designed to reduce wall friction.

3.4 The drag reduction property of the as-prepared surface

In order to estimate the drag reduction property, an experimental setup of the liquid/solid friction drag was reported [31]. Figure 6(a) shows the schematic that we used for testing the drag reduction efficiency of the as-prepared surfaces. A force sensor was introduced between the two sliding pairs to measure the friction drag between the flat flow and the fixed super hydrophobic surface. The samples with different contact angles were cut into samples of size 1.5 × 1.0 cm^2 and were fixed at the bottom of the force sensor. The copper nozzle with a caliber of 1.5 × 1.0 cm^2 was used to release the flat flow, which was provided by a water pump. The flowmeter was introduced to adjust the flow rate. The friction drag of the solid-liquid interface was transformed into an electric signal and collected by an external data acquisition system and then computed by a computer. The drag reduction properties of the superhydrophobic surface are measured thrice for the same flow rate. The average values were ultimately selected as the friction drag of the corresponding surface. Moreover, the friction drag was also measured under different flow rates to investigate the influence of the flow rate on the drag reduction performance. As shown in Fig. 6(b), the superhydrophobic surface has the lowest friction drag. The drag reduction ratio of the superhydrophobic surface is 30%–35% at low velocity. When the flow velocity was about 4.5 $m{\cdot}s^{-1}$, the drag reduction ratio reduced to 10%–20%. These results suggest that the flow velocity can affect the effect of the drag reduction. This is because the entrapped gas in the hydrophobic microstructures of a surface can also bepartially or completely removed by the interfacial shear induced by the flow. The drag reduction ratio results obtained by the experimental method are almost equal to the simulation results at low velocities.

4 Conclusions

In this study, an air bubble model was applied to simulate channel flow. The mechanism of drag reduction by using superhydrophobic surfaces was studied, and the effects of surface wettability and roughness on flow performance were analyzed. The superhydrophobic surface could trap bubbles, reducing the resistance of the

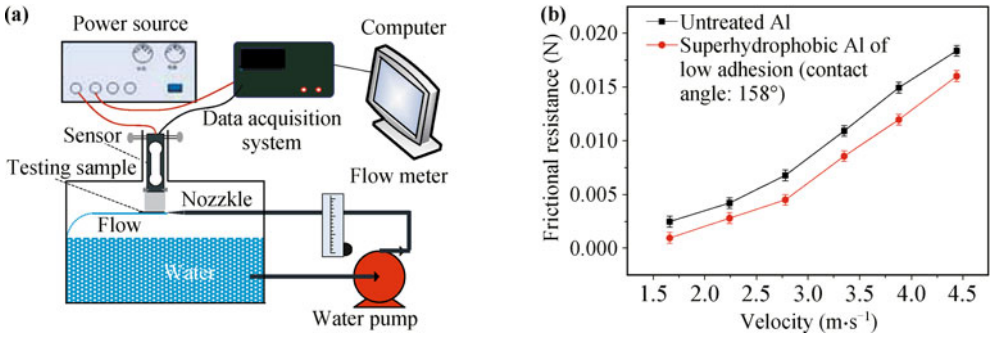

Fig. 6 **(a)** Schematic of the friction measurement. **(b)** Friction drag versus the velocity of the water flowing over surfaces.

surface. The conclusion is that the smaller the bubbles or the smoother the surface, the longer the slip length and the better the drag reduction effect. The numerical relationship between the surface contact angle and slip length was obtained according to the solid-liquid contact ratio as per the Cassie equation. When thesolid-liquid contact ratiodecreased from 90% to 10%, the surface friction is increased by 40% at low velocities.

Acknowledgements This work was supported by the National Basic Research Program of China (Grant No. 2012CB934104), the National Natural Science Foundation of China (Grant No. 61474034), Natural Science Foundation of Heilongjiang Province of China (NO. F201418), the Fundamental Research Funds for the Central Universities (Grant Nos. HIT.NSRIF.2014040 and HIT.NSRIF.2013040).

References

1. Y. L. Zhang, H. Xia, E. Kim, and H. B. Sun, Recent developments in superhydrophobic surfaces with unique structural and functional properties, *Soft Matter* 8(44), 11217 (2012)
2. C. H. Xue, S. T. Jia, J. Zhang, and J. Z. Ma, Large-area fabrication of superhydrophobic surfaces for practical applications: An overview, *Sci. Technol. Adv. Mater.* 11(3), 033002 (2010)
3. G. McHale, M. Newton, and N. Shirtcliffe, Immersed superhydrophobic surfaces: Gas exchange, slip and drag reduction properties, *Soft Matter* 6(4), 714 (2010)
4. Y. Zhao, Y. Song, W. Song, W. Liang, X. Jiang, Z. Tang, H. X. Xu, Z. X. Wei, Y. Q. Liu, M. H. Liu, L. Jiang, X. H. Bao, L. J. Wan, and C. L. Bai, Progress of nanoscience in China, *Front. Phys.* 9(3), 257 (2014)
5. N. P. Dasgupta and P. Yang, Semiconductor nanowires for photovoltaic andphotoelectrochemical energy conversion, *Front. Phys.* 9(3), 289 (2014)
6. P. Tao, W. Shang, C. Song, Q. Shen, F. Zhang, Z. Luo, N. Yi, D. Zhang, and T. Deng, Bioinspired engineering of thermal materials, *Adv. Mater.* 27(3), 428 (2015)
7. J. Wang, M. Liu, R. Ma, Q. Wang, and L. Jiang, In situ wetting state transition on micro- and nanostructured surfaces at high temperature, *ACS Appl. Mater. Interfaces* 6(17), 15198 (2014)
8. U. G. K. Wegst, H. Bai, E. Saiz, A. P. Tomsia, and R. O. Ritchie, Bioinspired structural materials, *Nat. Mater.* 14(1), 23 (2014)
9. W. Barthlott, T. Schimmel, S. Wiersch, K. Koch, M. Brede, M. Barczewski, S. Walheim, A. Weis, A. Kaltenmaier, A. Leder, and H. F. Bohn, The *Salvinia* paradox: Superhydrophobic surfaces with hydrophilic pins for air retention under water, *Adv. Mater.* 22(21), 2325 (2010)
10. S. Lyu, D. C. Nguyen, D. Kim, W. Hwang, and B. Yoon, Experimental drag reduction study of super-hydrophobic surface with dual-scale structures, *Appl. Surf. Sci.* 286, 206 (2013)
11. J. Cui, W. Li, and W. Lam, Numerical investigation on drag reduction with superhydrophobic surfaces by lattice-Boltzmann method, *Comput. Math. Appl.* 61(12), 3678 (2011)
12. Y. Gan, A. Xu, G. Zhang, and Y. Li, Physical modeling of multiphase flow via lattice Boltzmann method: Numerical effects, equation of state and boundary conditions, *Front. Phys.* 7(4), 481 (2012)
13. K. Fukagata, N. Kasagi, and P. Koumoutsakos, A theoretical prediction of friction drag reduction in turbulent flow by superhydrophobic surfaces, *Phys. Fluids* 18(5), 051703 (2006)
14. E. Lauga and H. A. Stone, Effective slip in pressure-driven Stokes flow, *J. Fluid Mech.* 489, 55 (2003)
15. J. Davies, D. Maynes, B. W. Webb, and B. Woolford, Laminar flow in a microchannel with superhydrophobic walls exhibiting transverse ribs, *Phys. Fluids* 18(8), 087110 (2006)
16. Y. P. Cheng, C. J. Teo, and B. C. Khoo, Microchannel flows with superhydrophobic surfaces: Effects of Reynolds number and pattern width to channel height ratio, *Phys. Fluids* 21(12), 122004 (2009)
17. J. Yang, J. Duan, D. Fornasiero, and J. Ralston, Very small bubble formation at the solid-water interface, *J. Phys. Chem. B* 107(25), 6139 (2003)
18. J. Wang, H. Chen, T. Sui, A. Li, and D. Chen, Investigation on hydrophobicity of lotus leaf: Experiment and theory, *Plant Sci.* 176(5), 687 (2009)
19. S. R. German, X. Wu, H. An, V. S. J. Craig, T. L. Mega, and X. Zhang, Interfacial nanobubbles are leaky: Permeability of the gas/water interface, *ACS Nano* 8(6), 6193 (2014)
20. X. Zhang, A. Quinn, and W. A. Ducker, Nanobubbles at the interface between water and a hydrophobic solid, *Langmuir* 24(9), 4756 (2008)
21. J. Wang, B. Wang, and D. Chen, Underwater drag reduction by gas, *Friction* 2(4), 295 (2014)
22. K. Mohanarangam, S. C. P. Cheung, J. Y. Tu, and L. Chen, Numerical simulation of micro-bubble drag reduction using population balance model, *Ocean Eng.* 36(11), 863 (2009)
23. P. P. Modi and S. Jayanti, Pressure losses and flow maldistribution in ducts with sharp bends, *Chem. Eng. Res. Des.* 82(3), 321 (2004)
24. B. M. Borkent, S. M. Dammer, H. Schonherr, G. J. Vancso, and D. Lohse, Superstability of surface nanobubbles, *Phys. Rev. Lett.* 98(20), 204502 (2007)
25. P. Joseph, C. Cottin-Bizonne, J. M. Benoit, C. Ybert, C. Journet, P. Tabeling, and L. Bocquet, Slippage of water past superhydrophobic carbon nanotube forests in microchannels, *Phys. Rev. Lett.* 97(15), 156104 (2006)
26. A. Steinberger, C. Cottin-Bizonne, P. Kleimann, and E. Charlaix, High friction on a bubble mattress, *Nat. Mater.* 6(9), 665 (2007)

27. C. Lee and C. J. Kim, Maximizing the giant liquid slip on superhydrophobic microstructures by nanostructuring their sidewalls, *Langmuir* 25(21), 12812 (2009)
28. J. Hyväluoma and J. Harting, Slip flow over structured surfaces with entrapped microbubbles, *Phys. Rev. Lett.* 100(24), 246001 (2008)
29. S. Richardson, No-slip boundary condition, *J. Fluid Mech.* 59(04), 707 (1973)
30. K. M. Jansons, Determination of the macroscopic (partial) slip boundary condition for a viscous flow over a randomly rough surface with a perfect slip microscopic boundary condition, *Phys. Fluids* 31(1), 15 (1988)
31. Y. Wang, X. W. Liu, H. F. Zhang, and Z. P. Zhou, Superhydrophobic surfaces created by a one-step solution-immersion process and their drag-reduction effect on water, *RSC Advances* 5(24), 18909 (2015)